NRC Research Press

ARTICLE

Study of heterostructures of Cu_3BiS_3–buffer layer measured by Kelvin probe force microscopy measurements (KPFM)[1]

F. Mesa and D. Fajardo

Abstract: The interface formed between Cu_3BiS_3 thin films and the buffer layer is a potentially limiting factor to the performance of solar cells based on Al/Cu_3BiS_3/buffer heterojunctions. The buffer layers of ZnS and In_2S_3 were grown by co-evaporation, and tested as an alternative to the traditional CdS deposited by chemical bath deposition. From the Kelvin probe force microscopy measurements, we found the values of the work function of ZnS, In_2S_3, and CdS, layers deposited into Cu_3BiS_3. Additionally, different electronic activity was found for different grain boundaries (GBs), from studies under illumination, we also found the net doping concentration and the density of charged GB states for Cu_3BiS_3 and Cu_3BiS_3/CdS.

PACS Nos.: 68.55.J–, 07.79.Lh, 73.30.+y.

Résumé : L'interface formée entre Cu_3BiS_3 couches minces et la couche tampon est un facteur limitant potentiel à la performance des cellules solaires à base de heterojuntions de Al/Cu_3BiS_3/buffer. Les couches tampons de ZnS et In_2S_3 ont été cultivées par co-évaporation, et testés comme une alternative aux traditionnels CdS déposés par la CDB. A partir des mesures de microscopie à force Kelvin probe, nous avons trouvé les valeurs de la fonction de travail de ZnS, In_2S_3 et des CdS, des couches déposées sur Cu_3BiS_3. En outre, l'activité électronique différent a été trouvée pour les joints de grains (GBs) différents, à partir d'études de moins de éclairage, aussi nous avons constaté que la concentration de dopage net et la densité de charge états GBs pour Cu_3BiS_3 et Cu_3BiS_3/CdS.

1. Introduction

Recently, several studies have focused on obtaining new semiconducting materials that have good optoelectronic properties [1–4]. However, currently most semiconductors used for photovoltaic applications are Cu(In, Ga)Se_2 and CdTe [5–6], because these have reached the maximum conversion efficiency [7]. In this search we highlight Cu(In,Ga)S, Cu_3BiS_3, and $AgInS_2$ as an absorbent layer in solar cells [8–10], because elements such as Se, Te, and Cd are not included within their structures, which is beneficial because of the toxicity of these elements in high concentrations.

Moreover, the buffer layer that is usually composed of CdS [11] is also studied. Alternatively, a new study has suggested layers of In_2S_3, ZnS, ZnO-i, and $Zn_{1-x}Mg_xO$, which have been deposited by different techniques, such as coevaporation, radio frequency sputtering, atomic layer deposition, spray ions layer gas reaction, spray pyrolysis, and chemical bath deposition [12–14]. However, it has been demonstrated that the electronic properties of the absorbent layer in solar cells strongly depend on the technique used to grow buffer layers [15].

Electronic properties have a very important aspect, because they have achieved considerable photovoltaic conversion efficiency despite the existence of many grain boundaries (GBs) [16]. On the surface of a pure $CuGaSe_2$ film area analysis has been made of the differences in work functions with crystal orientation, which has shown that for many grains there are electronic charges [17, 18]. In particular, studies under illuminated conditions have provided information about the charging and discharging of surface and defect states through the measurement of the surface photovoltage.

In this work, the topographic and electronic properties of Cu_3BiS_3 and the effect of the layers of CdS, ZnS, and In_2S_3 thin films on Cu_3BiS_3 were studied, measured by Kelvin probe force microscopy (KPFM). These layers were deposited through coevaporation and chemical bath deposition. However, In_2S_3 is very attractive because it has been proposed as a new buffer layer in solar cells [19] as a structure having TCO/In_2S_3/Cu_3BiS_3/Al.

2. Experimental

The Cu_3BiS_3 thin films were deposited on soda-lime substrates through the processes of evaporation of Bi and Cu metal precursors under a sulphur atmosphere (sulphurization) in two stages and keeping the substrate temperature at 300 °C during the entire process. In the first stage, Bi is evaporated leading to a Bi_xS_y layer. In the second stage Cu is co-evaporated. The second stage is co-evaporation of Cu, creating a Cu_xS_y layer that chemically reacts with the Bi_xS_y layer, resulting in the formation of the compound Cu_3BiS_3. Al contacts were used for analysis by KPFM [20]. CdS thin films were deposited by chemical bath deposition on Cu_3BiS_3 thin films. The thickness of the films was approximately 80 nm. For specific experimental conditions see ref. 21; the thin film formation follows chemical reaction

$$[Cd^{2+}]_{(ac)} + NH_2SCNH_{2(ac)} + OH^- \leftrightharpoons [CdS]_{film} + NCNH_2 + H_2O \quad (1)$$

ZnS films were grown by co-evaporation of Zn into an atmosphere of S, which is evaporated by keeping the substrate temperature at 250 °C. A thickness monitor (Maxtec TM-400) with a quartz crystal sensor, was used to measure the deposition rate of Zn. The thickness of the films was ~120 nm. In ref. 22 the details of the procedure used to prepare the ZnS films are given.

On the other hand, In_2S_3 samples were deposited through the co-evaporation of In and S on a substrate heated at temperatures

Received 20 October 2013. Accepted 22 May 2014.

F. Mesa and D. Fajardo. Unidad de Estudios Universitarios, Universidad del Rosario, Cra. 24 No 63C-69 Bogotá-Colombia.
Corresponding author: Dalila Fajardo (e-mail: fgmesar@unal.edu.co, dalila.fajardo@urosario.edu.co).

[1]This paper was presented at the 25th International Conference on Amorphous and Nanocrystalline Semiconductors (ICANS25).

Fig. 1. (*a*) Topography, (*b*) work function profile between GBs, (*c*) profile of CPD at GB of Cu_3BiS_3 thin films. (Mapped as dark areas.)

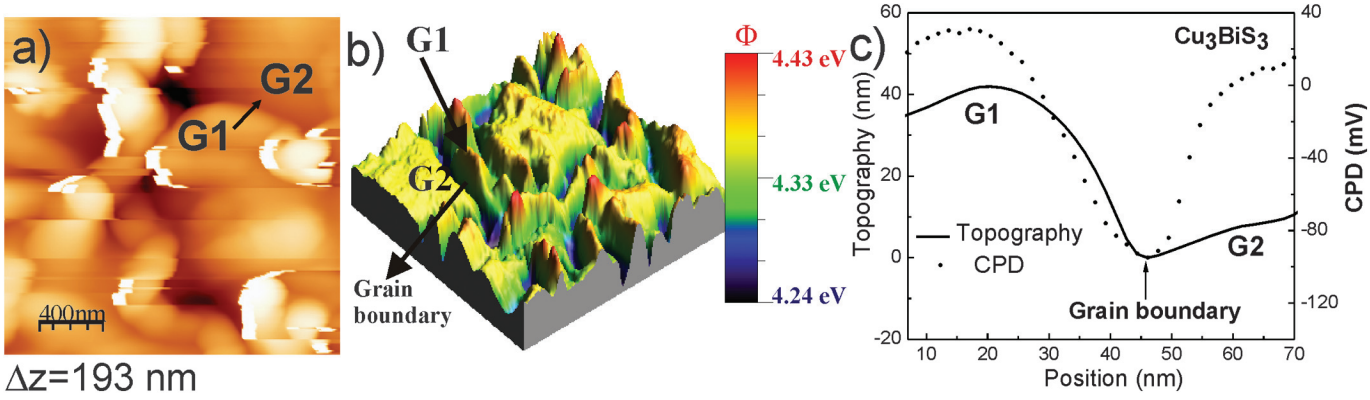

Fig. 2. (*a*) Cu_3BiS_3/CdS system topography, (*b*) changes in the work function in the GB, and (*c*) work function profile along two grains.

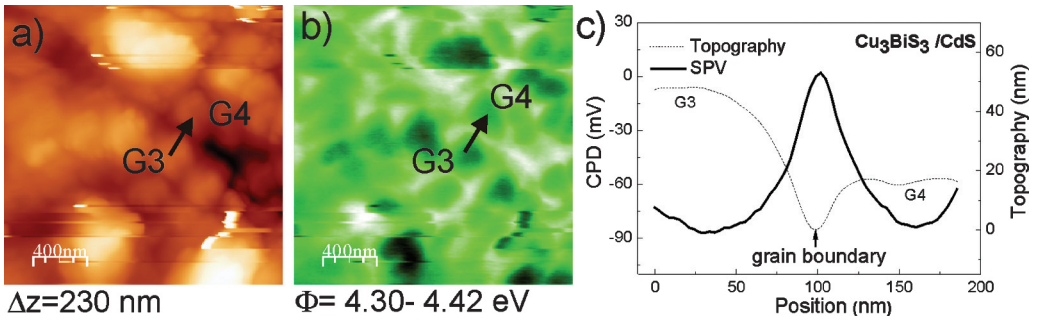

around 300 °C. The deposition system configuration has the same components aforementioned for the manufacturing of films of ZnS. The thickness of the films was ~150 nm. Finally, the aluminum contacts were deposited by sputtering DC magnetron. In ref. 23 details of the same procedure used to prepare the Mo films are given.

The KPFM measurements were accomplished by means of modified Omicron ultrahigh vacuum AFM/STM operating at a base pressure < 10^{-10} mbar, using the amplitude modulation technique (AM mode). We used PtIr-coated cantilevers (nanosensors) with an initial resonance frequency of ~75 kHz, measuring the contact potential difference (CPD) using the second resonance mode at ~450 kHz. We obtained an energy resolution of 5 meV using ac-voltages as low as 100 mV. The lateral resolution of the contact potential signal was determined to be approximately 20 nm. KPFM was performed in ultrahigh vacuum to determine the surface morphology and the surface photovoltage, which was converted to a work function using a calibration of the tip with a curvature radius of 5 nm on a graphite sample [24, 25].

3. Results and discussion

Because any contamination can modify the results of the KPFM, KPFM images were taken in an ultrahigh vacuum 10^{-11} mbar. Figures 1*a* and 1*b* show the difference in morphology and work function for two different regions at GB (G_1 and G_2), Fig. 1*c* shows changes in topography (solid line) and in CPD (dotted line) at GB between G_1 and G_2 of Cu_3BiS_3 thin films. The topography of Cu_3BiS_3 polycrystalline samples exhibit a typical granular structure with the corresponding distribution of the work function measured in the dark. This work function presents variations between –110 and 78.4 meV (defined by the CPD). However, in Fig. 1*b* the variation of CPD was further observed with a distribution of work functions, it is best observed in the histogram shown in Fig. 4*a*. Different peaks in the distribution can well be fitted by a Gauss distribution varying between Φ = 4.34 and 4.46 eV and a full width at half maximum varying between approximately 0.02 and 0.1 eV, when it is treated with HN_3. The results revealed that the work function obtained is of 4.36 ± 0.04 eV (determined in area $A = 2\ \mu m \times 2\ \mu m$), which takes an average value of the entire distribution in the histogram, presented different values of Φ, which cannot be explained by sample homogeneity, giving rise to a nonuniform distribution.

Alternatively, to analyze the behavior of the electronic structure of the GBs of Cu_3BiS_3, following the model proposed by Seto [26] of Si, which explains the drop in the work function by the presence of intergrain states positively charged. Applying this model, can determine the net concentration of dopant impurities (P_{net}) of Cu_3BiS_3 and the charge density in the states of GB [18]

$$P_{net} = \frac{2\varepsilon_0\varepsilon\Delta\Phi_{gb}}{e^2w^2} \quad (2)$$

$$P_{gb} = \frac{1}{e}\sqrt{8\varepsilon_0\varepsilon P_{neta}\Delta\Phi_{gb}} \quad (3)$$

where $\varepsilon \sim 10$ is the electric permeability of the absorbent layer, ε_0 is the dielectric constant and e is the elemental charge, this model was already used by Fuertes Marrón [18] for $CuGaSe_2$ thin films. Using the experimentally obtained results for the potential drop $\Delta\Phi/e = -91$ meV and the space-charge region width $w \approx 54.3$ nm, we obtain the net doping concentration $P_{net} = 3.86 \times 10^{16}$ cm^{-3} and the density of charged grain-boundary states $P_{gb} = 4.19 \times 10^{11}$ cm^{-2}, this is according to results obtained by Hall effect measurements on Cu_3BiS_3 absorbers [20].

Figure 2 shows a similar study of the Cu_3BiS_3–CdS system where the top layer is CdS, Fig. 2*c* shows changes in topography (solid line) and CPD (dotted line) at GB between G_3 and G_4, in this system

Fig. 3. Scanning electron microscope images of (*a*) Cu_3BiS_3, (*b*) Cu_3BiS_3/CdS, (*c*) Cu_3BiS_3/ZnS, and (*d*) Cu_3BiS_3/In_2S_3 system analyzed.

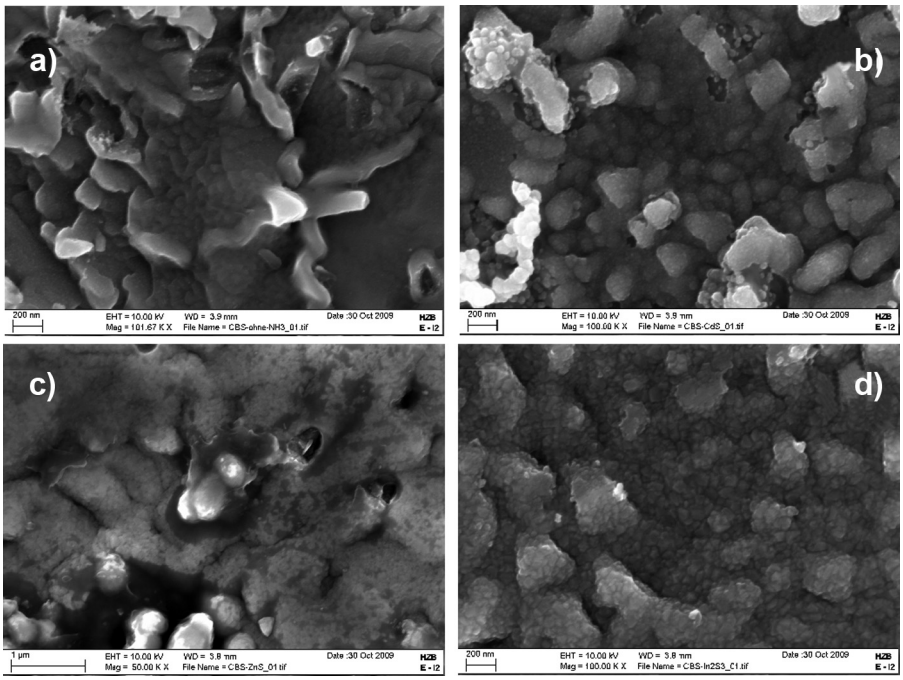

Fig. 4. Histograms showing the work function distribution obtained by KPFM for: (*a*) Cu_3BiS_3; (*b*) Cu_3BiS_3, cleaning with ammonia; (*c*) Cu_3BiS_3/ZnS system; (*d*) Cu_3BiS_3/In_2S_3 system; and (*e*) Cu_3BiS_3/CdS system. (*f*) Work functions obtained for different samples obtained in dark and illuminated conditions.

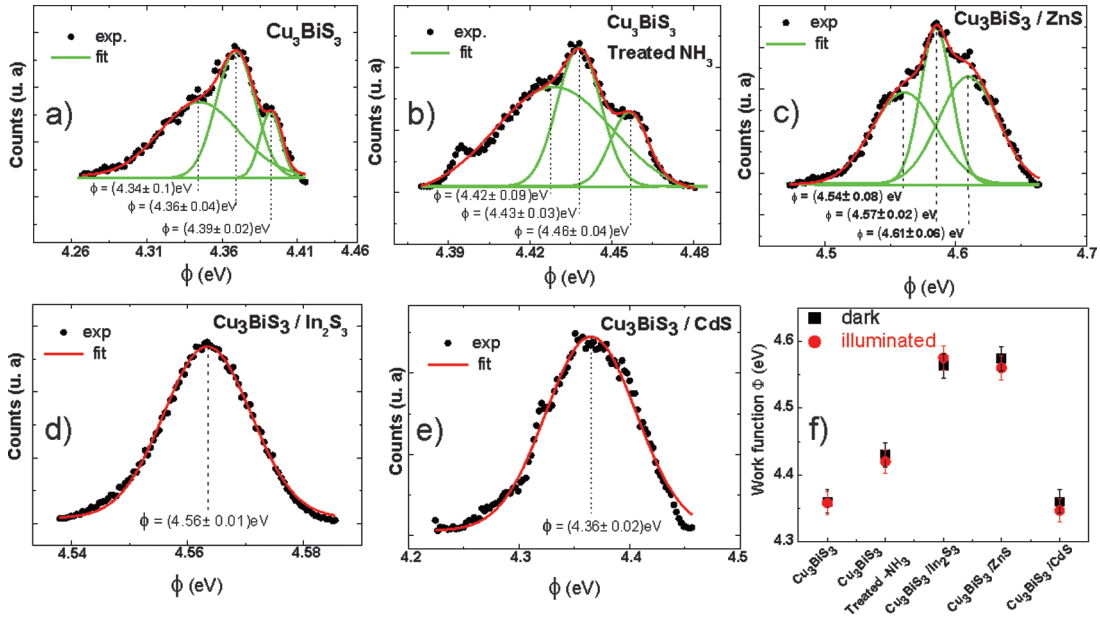

the CPD profile is different to the Cu_3BiS_3 absorber layer, it presents a peak at GB contrary to Cu_3BiS_3 absorber, however, the work function takes on smaller values into the grain, which can be associated with sulphur vacancy in CdS induced by sulphur diffusion from CdS interior particle to GB, the sulphur diffusion passivate states at GBs. It was found that the CdS net doping concentration was $N_{net} = 2.9 \times 10^{16}$ cm^{-3} and the density of charged GB states was $N_{gb} = 3.2 \times 10^{11}$ cm^{-2}. Sadewasser et al. [27], reported that these differences in magnitude of the work-function drop at GBs and doping concentrations estimated from the top and rear surfaces of this material may have their origin not only in the type of technology employed, but also and perhaps more significantly in the type of process followed for the film growth, particularly those leading to composition gradients within the layer thickness, such as sequential or multistage processes.

To obtain information regarding the homogeneity and topography of the samples with Cu_3BiS_3/buffer structure, scanning electron microscope measurements were taken, shown in Fig. 3. Figure 3*a* shows the thin film of Cu_3BiS_3 on top of the glass substrate. Figures 3*b*, 3*c*, and 3*d* show the structures of Cu_3BiS_3/CdS,

Cu_3BiS_3/ZnS and Cu_3BiS_3/In_2S_3, respectively. Starting with the scanning electron microscope images, it can be observed that the Cu_3BiS_3 samples (Fig. 3*a*) grow presenting a scale-type formation, with very irregular and inhomogeneous grain size, showing fractures on the topmost region [28], which were confirmed in Fig. 1; while depositing buffer layers on the Cu_3BiS_3, a formation of one substructure made up of much smaller grains (in the order of nanometres) which grow preferentially in the intergrain region, can be observed. This effect makes the electronic properties of the material change, which were determined by way of KPFM. Additionally, samples with Cu_3BiS_3/In_2S_3 structure present the highest homogeneity, making this buffer layer an optimum layer that allows the defective states of Cu_3BiS_3 [20] to be passivated.

Cu_3BiS_3 samples exhibited a Bi_2O_3 layer when exposed to the atmosphere, which is clearly evidenced in previous studies [29]. It is also clear that the NH_3 etch removes these oxide peaks to a large extent. For surface cleaning, the sample was etched in a 3% aqueous NH3 solution for 150 s at room temperature and transferred through air into the ultrahigh vacuum system within less than 5 min. In KPFM, surface cleaning is very important to obtain correct electronic information; for this study, the effect of Cu_3BiS_3 work function on buffer layer (passivation effect [20]) cleaning procedure was realized, three different buffer layers were deposited on Cu_3BiS_3 absorbers by chemical bath deposition and coevaporation methods, cleanness procedure with ammonia was done. Figure 4 shows histogram profiles of work functions for Cu_3BiS_3, Cu_3BiS_3 cleaning with ammonia, Cu_3BiS_3/In_2S_3, Cu_3BiS_3/ZnS, and Cu_3BiS_3/CdS, and work functions obtained under dark and illuminated conditions. It was found that profile distribution of work functions for Cu_3BiS_3 and Cu_3BiS_3 cleaning with ammonia (Figs. 4*a* and 4*b*) can be represented by Gaussian superposition distribution; morphological analysis (not shown) does not change at all between as-grown Cu_3BiS_3 and Cu_3BiS_3 cleaning with ammonia, but an increase in surface photovoltage value was observed for Cu_3BiS_3 cleaning with ammonia at $\Phi = 4.43 \pm 0.03$ eV. Work function for Cu_3BiS_3 and Cu_3BiS_3 cleaning with ammonia shows a clear distinction between the values for different facets of Cu_3BiS_3 crystallites, the number of different peaks obtained from the histogram correspond to distinct Φ-value of each specific facet [25]. The same result is obtained to Cu_3BiS_3/ZnS system (Fig. 4*c*), where the work function increase to $\Phi = 4.57 \pm 0.02$ eV and histogram profile can be well fitted by Gaussian superposition distribution.

Different results are obtained for Cu_3BiS_3/In_2S_3 and Cu_3BiS_3/CdS systems (Figs. 4*d* and 4*f*); a single peak in the distribution that can be well fitted by a Gauss distribution with a maximum at $\Phi = 4.56 \pm 0.01$ eV for Cu_3BiS_3/In_2S_3 and at $\Phi = 4.36 \pm 0.02$ eV for a Cu_3BiS_3/CdS system; these results indicate that nonelectronic uniformity on as-grown Cu_3BiS_3 is eliminated by deposition of buffer layer on absorber; single peak in histogram profiles (Figs. 4*d* and 4*e*) indicates that the electronic uniformity of Cu_3BiS_3 surface is improved, buffer layer can passivate the GBs and different states present on Cu_3BiS_3 surface making electronic distribution of work function completely uniform.

In contrast, for photovoltaic applications, the effect of sample illumination presents an important source of information in the characterization of samples. Illumination with super band gap light will cause generation of electron–hole pairs that can be separated in internal fields of the semiconductor structure. This surface potential can be spatially resolved with the KPFM; Fig. 4*f* shows work functions obtained in dark and illuminated conditions for all samples studied; for the Cu_3BiS_3/In_2S_3 system the illuminated work function value is higher than illuminated work functions for Cu_3BiS_3, Cu_3BiS_3 cleaning with ammonia Cu_3BiS_3/ZnS and Cu_3BiS_3/CdS, this increment in work functions after illumination of the sample can be associated with passivation of Cu_3BiS_3 surface states by In_2S_3 deposition; additionally, because In_2S_3 presents higher state density at its surface than Cu_3BiS_3 surface, a big band bending occurs at the surface.

4. Conclusion

KPFM was analyzed for topographic and electronic behavior of Cu_3BiS_3 compound. The nonuniform distribution of the grains revealed that the work function takes different values in the sample. However, when using the structure Al/Cu_3BiS_3/buffer evidenced an improvement, which indicates that electronic uniformity of Cu_3BiS_3 surface is improved, buffer layer can passivate the GBs and different states present on Cu_3BiS_3 surface making the electronic distribution of the work function completely uniform.

Acknowledgements

This work was supported by COLCIENCIAS, Universidad Nacional de Colombia and Universidad del Rosario. Thanks to S. Sadawasser and G. Gordillo for their support in the interpretation and growth of the samples.

References

1. C. Pang, B. Yan, L. Liao, B. Liu, Z. Zheng, T. Wu, H. Sun, and T. Yu. Nanotechnology, **21**(46), 465706 (2010). doi:10.1088/0957-4484/21/46/465706.
2. C.C. Tseng, J.H. Hsieh, and W. Wu. Thin Solid Films, **519**, 5169 (2011). doi:10.1016/j.tsf.2011.01.081.
3. D. Kim. Displays, **31**, 155 (2010). doi:10.1016/j.displa.2010.05.002.
4. K. Yamada, N. Hoshino, and T. Nakada. Sci. Tech. Adva. Mater. **7**, 42 (2006). doi:10.1016/j.stam.2005.11.016.
5. I.M. Dharmadasa. Curr. Appl. Phy. **9**, Supplement e2–e6 (2009). doi:10.1016/j.cap.2008.12.021.
6. F. Couzinié-Devy, N. Barreau, and J. Kessler. Prog. Photovolt: Res. Appl. **19**, 527 (2011). doi:10.1002/pip.1079.
7. M. Green, K. Emery, Y. Hishikawa, W. Warta, and D. Dunlop. Prog. Photovolt: Res. Appl. **20**, 606 (2012). doi:10.1002/pip.2267.
8. S.J. Park, J.W. Cho, J.K. Lee, K. Shin, J.H. Kim, and B.K. Min. Prog. Photovolt: Res. Appl. **22**, 122 (2013). doi:10.1002/pip.2354.
9. F. Mesa, A. Dussan, and G. Gordillo. Physica B, **404**, 5227 (2009). doi:10.1016/j.physb.2009.08.302.
10. K.W. Cheng and P.H. Liu. Sol. Ener. Mater. Sol. Cells, **95**, 1859 (2011). doi:10.1016/j.solmat.2011.02.008.
11. N. Yavuz, S.A. Yuksel, A. Karsli, and S. Gunes. Sol. Ener. Mater. Sol. Cells, **116**, 224 (2013). doi:10.1016/j.solmat.2013.04.018.
12. Z. Gao, J. Liu, and H. Wang. Mater. Sci. Semicond. Process. **15**, 187 (2012). doi:10.1016/j.mssp.2012.02.004.
13. M.S. Daranfed, A. Aida, and H. Hafdallah. Lekiket Thin Solid Films, **518**, 1082 (2009). doi:10.1016/j.tsf.2009.03.227.
14. G.J. Fang, D. Li, B.L. Yao, and X. Zhao. J. Cryst. Growth, **258**, 310 (2003). doi:10.1016/S0022-0248(03)01505-7.
15. U. Rau, K. Taretto, and S. Siebentritt. Appl. Phys. A, **96**, 221 (2009). doi:10.1007/s00339-008-4978-0.
16. M. Hafemeister, S. Siebentritt, J. Albert, M. Lux-Steiner, and S. Sadewasser. Phys. Rev. Lett. **104**, 196602 (2010). doi:10.1103/PhysRevLett.104.196602. PMID:20866985.
17. H. Mönig, Y. Smith, R. Caballero, C. Kaufmann, I. Lauermann, M. Lux-Steiner, and S. Sadewasser. Phys. Rev. Lett. **105**, 116802 (2010). doi:10.1103/PhysRevLett.105.116802.
18. D.F. Marrón, A. Meeder, S. Sadewasser, R. Würz, C.A. Kaufmann, T. Glatzel, T. Schedel-Niedrig, and M.C. Lux-Steiner. J. Appl. Phys. **97**, 094915 (2005). doi:10.1063/1.1891274.
19. F. Mesa, A. Dussan, J. Sandino, and H. Lichte. J. Nanopart. Res.**14**, 1054 (2012). doi:10.1007/s11051-012-1054-7.
20. F. Mesa, G. Gordillo, T. Dittrich, K. Ellmer, R. Baier, and S. Sadewasser. Appl. Phys. Lett. **96**, 082113 (2010). doi:10.1063/1.3334728.
21. P.C. Rieke and S. Bentjen. Chem. Mater. **5**, 43 (1993). doi:10.1021/cm00025a012.
22. E. Romero, W. Vallejo, and G. Gordillo. Proc. 33rd IEEE Photovoltaic Specialist Conference, San Diego, USA (2008).
23. G. Gordillo, F. Mesa, and C. Calderón. Braz. J. Phys. **36**, 982 (2006). doi:10.1590/S0103-97332006000600049.
24. C. Sommerhalter, T.W. Matthes, T. Glatzel, A. Jäger-Waldau, and M. Lux-Steiner. Appl. Phys. Lett. **75**, 286 (1999). doi:10.1063/1.124357.
25. S. Sadewasser and T. Glatzel. Phys. Rev. Lett. **98**, 269701 (2007). doi:10.1103/PhysRevLett.98.269701. PMID:17678136.
26. J.Y.W. Seto. J. Appl. Phys. **46**, 5247 (1975). doi:10.1063/1.321593.
27. S. Sadewasser, T. Glatzel, S. Schuler, S. Nishiwaki, R. Kaigawa, and M.C. Lux-Steiner. Thin Solid Films, **257**, 431 (2003).
28. N. Gerein and J. Haber. Chem. Mater. **18**, 6297 (2006). doi:10.1021/cm061453r.
29. F. Mesa, W. Chamorro, W. Vallejo, R. Baier, T. Dittrich, A. Grimm, M. Lux-Steiner, and S. Sadewasser. Beilstein J. Nanotechnol. **3**, 277 (2012). doi:10.3762/bjnano.3.31. PMID:22497001.